Catalysis Today 156 (2010) 198–207

Contents lists available at ScienceDirect

Catalysis Today

journal homepage: www.elsevier.com/locate/cattod

Application of temperature modified titanate nanotubes for removal of an azo dye from water in a hybrid photocatalysis-MD process

Sylwia Mozia*

West Pomeranian University of Technology, Institute of Chemical and Environment Engineering, Pułaskiego 10, 70-322 Szczecin, Poland

ARTICLE INFO

Article history:
Available online 15 March 2010

Keywords:
Titanate nanotubes
Photocatalytic membrane reactor
PMR
Photocatalysis
Membrane distillation

ABSTRACT

The presented studies have focused on application of modified titanate nanotubes (TNTs) for decomposition of Acid Red 18 in water. The TNTs were prepared via hydrothermal method. The post-treatment of TNTs was carried out by calcination of the as-received nanotubes at temperatures of 400–700 °C. The photocatalytic experiments revealed that the most active towards AR18 decomposition were TNTs calcinated at 600 °C (TNT600). However, the photocatalytic activity of the calcinated titanate nanotubes, regardless of the annealing temperature applied was found to be lower than that of P25. In the second step of the investigations, the TNT600 were applied for degradation of AR18 in a photocatalytic membrane reactor coupling photocatalysis with membrane distillation. The effect of photocatalyst loading on the effectiveness of degradation of AR18 was especially investigated. After 5 h of irradiation the amount of AR18 was lowered for ca. 67, 80 and 97% for TNT600 loadings of 0.1–0.5 g/dm^3, respectively. The mineralization of the organics was significantly lower than the decolorization of the solution. The amount of TOC after 5 h of the experiment decreased for 20, 27 and 57%, for 0.1–0.5 g TNT600/dm^3, respectively. Amongst products and by-products of AR18 photodegradation organic acids (formic, acetic and oxalic) and inorganic ions (nitrite, nitrate, ammonia and sulfate) were detected. The product of the hybrid process (distillate) was high quality water with conductivity in the range of 2.3–3 μS/cm.

1. Introduction

Over the last several years a great deal of interest has been focused on a new type of photocatalytic reactors, taking advantage of photodegradation of pollutants in water and membrane technology. These reactors, called photocatalytic membrane reactors (PMRs) seem to be a very promising method of solving problems concerning separation of photocatalyst as well as products and by-products of photodecomposition from the reaction mixture.

Photocatalytic membrane reactors exhibit some advantages with respect to conventional photoreactors, such as [1]: (I) confining of the photocatalyst in the reaction environment by means of the membrane; (II) control of a residence time of molecules in the reactor; (III) realization of a continuous process with simultaneous catalyst and products separation from the reaction environment. Moreover, application of a PMR instead of a conventional photoreactor allows avoiding some additional operations, such as coagulation–flocculation–sedimentation which are necessary in order to remove catalyst from the treated solution. One benefit from this is energy saving and reducing the size of installation. Another one is possibility of reusing of the photocatalyst in further runs, what is practically impossible when the conventional separation system composed of coagulation–flocculation–sedimentation steps is applied.

Most of the PMRs described in the literature combine photocatalysis with pressure driven membrane processes such as microfiltration (MF) [2–17], ultrafiltration (UF) [18–24] and nanofiltration (NF) [1,25–30]. However, when a catalyst in suspension is applied, the membrane fouling is observed, especially in case of MF and UF membranes. Moreover, the quality of permeate is not very high, because small molecules can pass easily through the membranes used, even in case of NF.

Recently new types of photocatalytic membrane reactors combining photocatalysis with dialysis [31] and pervaporation (PV) [32] have been described. In our earlier publications [33–40] we have presented a new type of PMR utilizing photocatalysis and direct contact membrane distillation (MD, DCMD). One of the main advantages of the above-mentioned configuration was high quality of the product (distillate). Moreover, no membrane fouling due to the presence of photocatalyst particles was observed.

TiO_2 is the most often used photocatalyst due to its considerable photocatalytic activity, high stability, non-environmental impact and low cost. Since Kasuga et al. [41,42] described a novel hydrothermal method for formation of titanate nanotubes (TNTs), the investigations on preparation and properties of these species have attracted attention of numerous researchers. Amongst various

* Tel.: +48 91 449 43 26; fax: +48 91 449 46 86.
E-mail addresses: sylwia.mozia@zut.edu.pl, sylwiam@ps.pl.

0920-5861/$ – see front matter © 2010 Elsevier B.V. All rights reserved.
doi:10.1016/j.cattod.2010.02.026

possible applications, including supports, ion-exchange, adsorption, dye sensitized solar cells, and others, photocatalysis seems to be of special interest. However, the data concerning the photocatalytic activity of the as-synthesized TNTs are inconsistent [43–53]. Yu et al. [44] investigated photocatalytic oxidation of acetone in air in the presence of TNTs synthesized hydrothermally at 150 °C for 48 h. The authors found that prior to calcination, the nanotubes showed no photocatalytic activity. Similar observations were published by Qamar et al. [45]. The researchers reported that the as-prepared nanotubes, with or without sodium content, showed no photocatalytic activities towards amaranth degradation. Baiju et al. [46] presented results on the photocatalytic degradation of Methylene Blue (MB) on a mixed nanobelts–nanotubes titanate obtained via hydrothermal method at 150 °C for 30 h. The authors found that the sample exhibited very high adsorptivity towards MB. However, the photocatalytic activity was very low. On the other hand, significant activity of titanate nanotubes towards HCHO degradation under UV light was reported by Nakahira et al. [48]. According to Xiao et al. [49], titanate nanotubes synthesized hydrothermally at 130 °C for 24 h revealed photocatalytic activity toward Rhodamine B (RhB) degradation with efficiency similar to that of P25. Photocatalytic activity of as-prepared TNTs towards Methylene Blue (MB) degradation and oxidation of NO to NO_2 was reported by Inagaki et al. [50]. Similarly, Geng et al. [51] observed photodegradation of MB in the presence of TNTs. Jiang et al. [52] found significant photocatalytic activity of TNTs during photodecomposition of Acid Red 3B. Moreover, the authors reported that TNTs washed with HCl solution were significantly more active than TNTs washed with water. Recently, Costa et al. [53] reported a considerable photocatalytic activity of titanate nanotubes during degradation of indigo carmine dye, although it was lower than that of anatase TiO_2. The inconsistencies in the reports on the photocatalytic activity of TNTs obtained by the hydrothermal method might result mainly from different precursors used (amorphous TiO_2, anatase, rutile, mixture of both phases, such as P25, etc.) and reaction conditions applied (temperature, time, etc.). Another reason might be that the obtained product contained unreacted anatase phase, from which the sample gained the photocatalytic activity.

Recently, different attempts to improve the photoactivity of TNTs have been made. They include post-thermal treatment, post-hydrothermal treatment, acid modification and others [43]. The literature data on the influence of post-thermal treatment on the photoactivity of TNTs are rather limited. However, most of the already published results suggest that calcination of TNTs significantly improves their photoactivity. For example, Lee et al. [54] found that TNTs with low sodium content calcinated at 300–600 °C exhibited high photoactivity towards decomposition of basic dye BV10; however, the reaction rate constants determined for P25 were higher. Qamar et al. [45] reported that titanate nanotubes calcinated at 500 °C were almost as active as P25 during photodecomposition of amaranth. According to Yu et al. [44] TNTs calcinated at 400 and 500 °C exhibited much higher activity towards degradation of acetone in air than P25.

Taking into consideration all the above-mentioned inconsistencies it seems to be important to continue the investigations on the photocatalytic properties of TNTs and products of their calcination. The presented research has been focused on the verification of the literature data concerning photocatalytic activity of the as-received TNTs and TNTs modified by post-thermal treatment. During the first part of the studies the thermal modification of titanate nanotubes obtained from TiO_2 P25 by hydrothermal method was conducted. The effect of different calcination temperatures on the photocatalytic activity of the temperature modified samples towards degradation of model azo dye Acid Red 18 (AR18) was investigated and compared to that of P25. In the second part of the research the effectiveness of the removal of AR18 from water in the photocatalytic membrane reactor coupling photocatalysis and MD was investigated. The effect of catalyst loading on the degradation rate of the dye and the permeate quality was especially determined.

2. Materials and methods

2.1. Preparation of TNTs

2.1.1. As-received TNTs

TNTs were synthesized using the hydrothermal method reported for the first time by Kasuga et al. [41,42], and later developed by others [43–57]. The main differences between the procedures used are the substrate type and concentration, NaOH and HCl concentrations, reactor volume as well as reaction time and temperature. However, the overall idea of the hydrothermal method is in every case similar to that presented by Kasuga et al. [41,42]. The procedure applied in this study was as follows. Commercial TiO_2 P25 (Evonik, former Degussa, Germany) was used as a starting material for TNTs preparation. The P25 consists of 75% of anatase and 25% of rutile. The BET surface area of P25 is ca. 50 m^2/g and the crystallite size of anatase is 25 nm (all data according to the manufacturer). 1.5 g of P25 was introduced to a Teflon-lined autoclave (70 cm^3) containing 60 cm^3 10 M NaOH. The suspension was ultrasonically treated for 1 h in order to allow good dispersion of TiO_2 particles in the reaction mixture. After that the autoclave was heated statically at 130 for 24 h. After the heat treatment the NaOH solution was decanted and the obtained precipitate was dispersed in 0.5 dm^3 of 0.1 M HCl. After 1 h the precipitate was separated from the HCl solution and dispersed again in 0.5 dm^3 of fresh 0.1 M HCl. After the next 2 h the precipitate was washed thoroughly with deionized water (Simplicity, Millipore) until the conductivity of washing solution reached the value of 1 μS/cm or less. Eventually, the precipitate was dried in air at 80 °C for 24 h. Such obtained titanate nanotubes were denoted later as "TNT-0".

2.1.2. Temperature modified TNTs

The as-received nanotubes (TNT-0) were calcinated in air for 1 h at different temperatures ranging from 400 to 700 °C (the samples are therefore denoted later as TNT400; TNT500; TNT600; TNT700). Heating rate was 10 °C/min. After calcination the samples were ground in an agate mortar and applied in the photocatalytic experiments.

2.2. Characterization of TNTs

Transmission electron microscopy (TEM) images were recorded using FEI Tecnai F20 microscope. Samples were prepared by dispersing the powder in acetone by ultrasonic treatment, and then dropping the suspension onto a copper grid (400 mesh). X-ray diffraction (XRD) analyses were performed using a powder diffractometer Philips X'Pert PRO (Cu Kα, 35 kV, 30 mA). TiO_2 anatase over rutile ratio was calculated from:

$$\text{anatase content } A = \frac{1}{1 + 1.26(I_R/I_A)} \quad (1)$$

where I_A and I_R are the diffraction intensities of the (1 0 1) anatase and (1 1 0) rutile crystalline phases at $2\theta = 25.3^\circ$ and 27.4°, respectively. The average anatase crystallite diameter D (nm) was determined using the Scherrer's equation:

$$D = \frac{K\lambda}{\beta \cos\theta} \quad (2)$$

where $K = 0.9$ is a shape factor for spherical particles, λ is the wavelength of the incident radiation (λ = 1.54056 Å), θ is half of the

diffraction angle (rad) and β is the line width at half-maximum height.

UV–vis/DR spectra were recorded using Jasco V530 spectrometer (Japan) equipped with the integrating sphere accessory for diffuse reflectance spectra. $BaSO_4$ was used as a reference.

Sodium content was determined using BWB-1 flame photometer (BWB Technologies, UK, Ltd.).

2.3. Evaluation of photocatalytic activity of thermally treated TNTs

In order to examine the effect of calcination temperature on the photoactivity of TNTs, the photocatalytic degradation of the model azo dye Acid Red 18 ($C_{20}H_{11}N_2Na_3O_{10}S_3$, AR18, Boruta-Kolor Sp. z o. o., Poland) was conducted. The initial concentration of AR18 was equal to 30 mg/dm^3. The photocatalytic reaction was carried out in a glass reactor containing 0.4 dm^3 of the model solution of AR18 and 0.3 g/dm^3 of a photocatalyst. The photocatalyst applied in these experiments were TNT-0, TNT400, TNT500, TNT600 and TNT700. Moreover, in order to compare the results, the photoactivity of P25 was determined.

The reaction mixture in the reactor was continuously stirred during the experiment. After 15 min in the dark, the solution was irradiated with UV-A light (Philips Cleo; 6× 20 W). The UV lamp was positioned above the reactor. After a defined time of irradiation the samples of reaction mixture were filtered through a 0.45 μm membrane filter and analyzed. The rate of AR18 photodegradation was estimated on the basis of (I) changes in dye concentration (λ_{max} = 507 nm, Jasco V530 spectrophotometer, Japan) and (II) total organic carbon (TOC) concentration ("Multi N/C 2000" analyzer, Analytik Jena, Germany).

On a basis of these experiments the thermally treated TNTs exhibiting the highest photoactivity towards AR18 degradation were selected and applied in the PMR combining photocatalysis and MD.

2.4. Degradation of Acid Red 18 in a photocatalytic membrane reactor

The hybrid photocatalysis-MD process was conducted in a laboratory-scale installation presented in Fig. 1. The main element of the system was a capillary module equipped with 9 polypropylene (PP) membranes (Accurel PP S6/2, d_{out}/d_{in} = 2.6/1.8 mm, Membrana GmbH, Wuppertal, Germany), having the effective area of 0.0127 m^2. The feed flowed inside the capillaries with a flow rate of 0.5 m/s, whereas the distillate flowed outside the capillaries with a flow rate of 0.18 m/s, respectively. The inlet temperature of the feed amounted to 63 °C for the reaction temperature (in the feed tank) of 60 °C, whereas the inlet temperature of distillate was 20 °C. The permeate flux measured for distilled water was 307 dm^3/(m^2 d) and remained constant during the experiments.

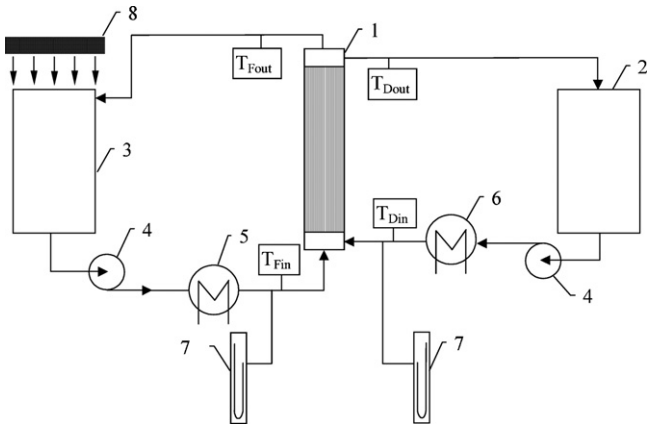

Fig. 1. Schematic diagram of the apparatus for the hybrid photocatalysis-MD process: (1) membrane module; (2) distillate tank; (3) feed tank (V = 2.9 dm^3); (4) pump; (5 and 6) heat exchangers; (7) manometers; (8) UV lamp; T_{Fin}, T_{Din}, T_{Fout}, T_{Dout}, inlet and outlet temperatures of feed and distillate, respectively.

At the beginning of the experiment the feed tank was filled with the model solution of AR18. The initial concentration of AR18 was equal to 30 mg/dm^3. After the solution reached the temperature of 60 °C, the photocatalyst (thermally treated TNTs) was added to the feed tank. The photocatalyst loading amounted to 0.1, 0.3 or 0.5 g/dm^3. The photocatalytic reaction was started after 15 min adsorption in the dark. The UV-A lamp (Philips Cleo; 6× 20 W) positioned above the feed tank was applied as a light source.

After a defined time of irradiation the samples of feed solution were filtered through a 0.45 μm membrane filter and analyzed. The rate of AR18 photodegradation was estimated on the basis of (I) changes in dye concentration (λ_{max} = 507 nm, Jasco V530 spectrophotometer, Japan), (II) total organic carbon (TOC) concentration ("Multi N/C 2000" analyzer, Analytik Jena, Germany), (III) conductivity (Ultrameter™ 6P, MYRON L COMPANY USA) and (IV) concentration of inorganic and organic ions being photoproducts of dye decomposition (Metrohm 850 Professional Ion Chromatograph (IC) equipped with Metrosep A Supp 5 250/4.0 and Metrosep C2 150/4.0 columns). The composition of distillate was determined on a basis of TOC, conductivity and ion concentrations measurements. Moreover, pH of the feed solution and distillate was measured.

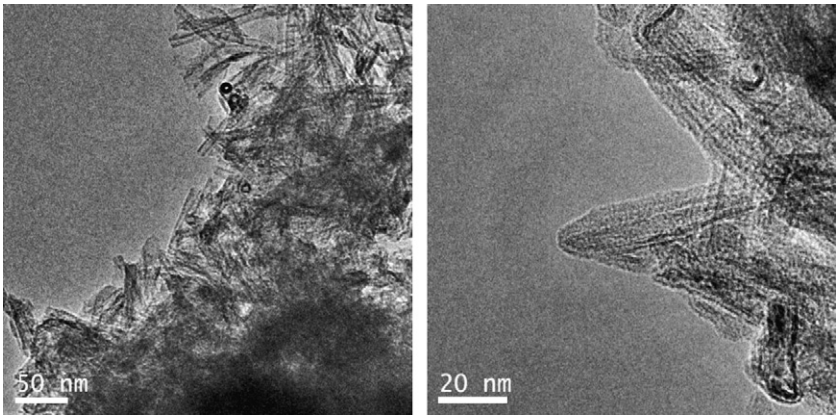

Fig. 2. TEM images of the as-received TNTs (TNT-0).

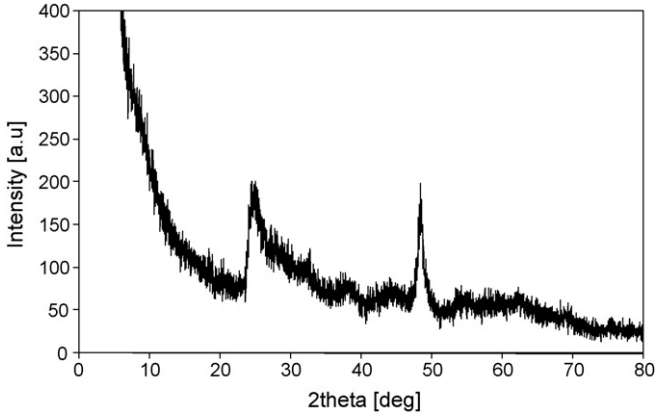

Fig. 3. XRD pattern of the as-received titanate nanotubes (TNT-0).

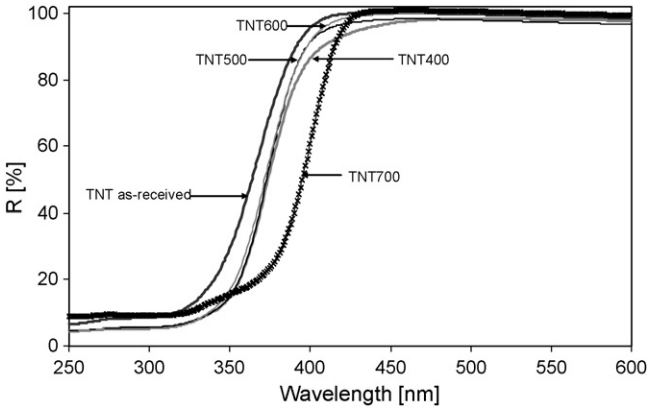

Fig. 4. UV–vis/DR spectra of the as-received (TNT-0) and thermally modified TNTs.

3. Results and discussion

3.1. Physico-chemical properties of as-received TNTs

Fig. 2 shows TEM images of the as-received titanate nanotubes (TNT-0). The nanotubes were scrolls with unequal number of walls on the two tube sides. The walls usually consisted of 3–4 layers. The distance between the layers, estimated from TEM measurements, was about 0.8 nm, what is in an agreement with the literature data [55–57]. The outer diameter of the nanotubes was in the range of 7.5–11.0 nm, whereas the inner diameter ranged from 4.5 to 6.5 nm.

In the XRD pattern of the TNT-0 (Fig. 3) three characteristic peaks positioned at 2θ 24, 28 and 48° can be observed. These peaks have been assigned to the diffraction of titanates such as $A_2Ti_2O_5{\cdot}H_2O$, $A_2Ti_3O_7$, and lepidocrocite titanates [43,58]. According to Zhang et al. [59] the most probable structure of TNTs is $Na_2Ti_2O_4(OH)_2$ (or $H_2Ti_2O_4(OH)_2$ in case of the replacement of Na^+ ions by H^+). These structures can be also presented as $Na_2Ti_2O_5{\cdot}H_2O$ and $H_2Ti_2O_5{\cdot}H_2O$, respectively. The $H_2Ti_2O_4(OH)_2$ exhibits an orthorhombic structure, having lattice parameters of $a = 19.26$, $b = 3.78$ and $c = 2.99$ Å [59]. Chen et al. [60] suggested that the structure of TNTs is $H_2Ti_3O_7$ (monoclinic, $a = 16.03$, $b = 3.75$, $c = 9.19$ Å and $\beta = 101.45°$). They explained that the interlayer spacing of $H_2Ti_3O_7$ is 0.78 nm, which is the same as that they observed in the nanotubes using SAED and HRTEM. Trititanate was also proposed as a structure of TNTs by Morgado et al. [61]. They found that the interlayer distance varied between 0.80 and 0.90 nm, i.e. was close to the d values of 0.78 and 0.84 nm in bulk trititanates $H_2Ti_3O_7$ and $Na_2Ti_3O_7$, respectively. Lepidocrocite-type titanate nanotubes with general formula $H_xTi_{2-x/4}\square_{x/4}O_4$ (orthorhombic, $a = 3.783$, $b = 18.735$ and $c = 2.978$ Å) was obtained by Ma et al. [62]. According to the authors the interlayer distance measured by ED was about 0.8 nm, which was lower than the d_{020} (0.93 nm) in lepidocrocite-type titanates. The difference has been attributed to the decrease of interlayer distance as a direct consequence of the loss of hydrated water during microscopic observations carried out under high vacuum. Taking into account this phenomenon, Ma et al. [62] concluded that the lepidocrocite-type titanate is more probable structure than trititanate. They have explained that the reported interlayer distance in $H_2Ti_3O_7$ of 0.78 nm, which was calculated on a basis of TEM and electron diffraction (ED) measurements cannot be accurate and is most likely underestimated due to the loss of hydrated water under vacuum. Similar conclusions were reported by others [55,56].

Taking into consideration the other peaks present in the XRD pattern of TNT-0 (Fig. 3), except from those identified at 24, 28 and 48° 2θ, it could be supposed that the structure of the TNT-0 is $H_2Ti_2O_5{\cdot}H_2O$ rather than $H_2Ti_3O_7$. According to the JCPDS card of $H_2Ti_2O_5{\cdot}H_2O$ (JCPDS 47-0124) the peaks characteristic for this compound are present at 24, 28, 33, 39, 46 and 48° 2θ. These peaks could be also identified in the diffraction pattern shown in Fig. 3. However, it should be remembered that the exact structure of TNTs is still a subject under debate [43].

The relative ratio of the intensities of the peaks at 24° and 28° 2θ can be used as a measure of sodium content. As shown in Fig. 3 the peak at 28° 2θ is much less intensive than the one at 24° 2θ. This suggests replacement of most of Na^+ ions by H^+ during washing with 0.1 M HCl [58]. The measurement of Na^+ ions concentration in the TNT-0 sample confirmed this supposition. Sodium content determined by flame photometry was 0.24 wt.%, which value shows that almost complete removal of Na^+ during washing was obtained.

On the basis of the UV–vis diffuse reflectance spectra (Fig. 4) the band gap energy (E_g) of the as-received TNTs (TNT-0) was calculated. The Kubelka–Munk method was applied in the calculations. The E_g values were determined from the $(F(R)h\nu)^{1/2}$ versus $h\nu$ plots, where $F(R) = (1 - R)/2R$ [63]. The absorption edge was found to be 378 nm, which value corresponds to the band gap energy of $E_g = 3.28$ eV. This value is significantly higher than that calculated for P25 (3.10 eV, 399 nm). Wang et al. [64] attributed the shift in the absorption edge (and, thus, higher E_g value) to the hydration and nano-size effect of TNTs.

3.2. Physico–chemical properties of thermally treated TNTs

The as-received TNTs (TNT-0) were modified by calcination at the temperatures of 400–700 °C in air atmosphere. The heat treatment changed significantly the properties of the nanotubes, as was found from XRD, UV–vis/DR and TEM measurements.

Fig. 5 presents the XRD patterns of the samples calcinated at different temperatures. It can be clearly seen that the phase compositions of the heat-treated samples differed significantly from that of the TNT-0 (Fig. 3). All the calcinated samples contained TiO_2; however, the treatment temperature affected the crystallographic structure of titania. In case of TNT400–TNT600 the only crystalline phase identified was anatase. Rising the calcination temperature up to 700 °C resulted in partial phase transformation from thermodynamically metastable anatase to the most stable form of TiO_2, rutile. The anatase and rutile contents in TNT700 calculated from (1) were 43 and 57%, respectively. A partial phase transformation from anatase to rutile at 700 °C in case of the thermally treated TNTs was also reported by Yu et al. [44]. In the diffraction pattern of TNT700 additional peaks which were identified as $Na_2Ti_6O_{13}$ could be observed. Similar results were obtained by Inagaki et al. [50] in case of TNTs annealed at 800 °C. The authors attributed the presence of $Na_2Ti_6O_{13}$ to the impurities remained in TNTs during their prepa-

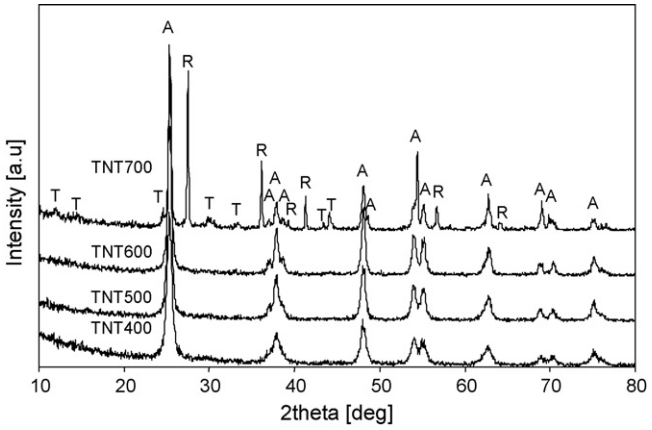

Fig. 5. XRD patterns of the thermally modified TNTs: A, anatase; R, rutile; T, $Na_2Ti_6O_{13}$.

ration. Torres–Martínez et al. [65] during their investigations on synthesis of $Na_2Ti_6O_{13}$ by sol–gel method found that single phase sodium hexatitanate was formed during annealing of the sample at 750 °C. Calcination at lower temperatures led to formation of TiO_2 or $Na_{0.23}TiO_2$. As was mentioned earlier, Na content in TNT-0 was 0.24 wt.%. The presence of sodium might explain formation of sodium hexatitanate at higher calcination temperatures.

From Fig. 5 it can be also seen that with increasing calcination temperature from 400 to 600 °C the peak intensities of anatase increased and the widths of these peaks decreased, indicating an improvement of the crystallinity of the samples. Indeed, the crystallite sizes of anatase, calculated from the Scherrer's equation (2) were equal to 12, 15, 18 and 25 nm for TNTs calcinated at 400–700 °C, respectively. An increase of the crystallite size of anatase with increasing the calcination temperature indicates aggregation of TiO_2 nanoparticles upon annealing. According to Su et al. [66] during the heat treatment of TiO_2, the dehydration takes place and as a result the crystals growth is observed.

Calcination of TNT-0 resulted in a destruction of a tubular structure. Fig. 6 shows the TEM images of the TNT400, TNT500, TNT600 and TNT700. It can be observed (Fig. 6a) that the sample calcinated at 400 °C contained a mixture of rod-shaped crystals and nanoparticles. Tubular structures of TNTs were difficult to be observed. As the temperature was rising up to 600 °C, the crystallization of rod-shaped and granular crystals was raised further, what is in agreement with the crystallite size determination from XRD data. The sample calcinated at 700 °C contained almost exclusively ball-shaped crystals with different sizes. The small crystals could be attributed to anatase, whereas the largest to rutile phase. From the TEM photographs it could be supposed that during annealing the nanotubular structures were transformed first to nanorods, which residues can be observed in TNT400–TNT600 samples. Further increase of the calcination temperature led to formation of anatase crystals, and then to phase transformation from anatase to rutile, which was associated with crystals growth. Similar observations were already reported in the literature [64,67].

Fig. 4 presents a comparison of the UV–vis diffuse reflectance spectra of the TNT-0 and TNTs calcinated at different temperatures. It can be observed that the spectra of the heat-treated TNTs are red shifted relative to that of the as-received TNTs. The shift in case of the samples prepared at 400–600 °C was about 6 nm, whereas for the TNT700–for ca. 37 nm. The band gap energy (E_g) of the calcinated TNTs was calculated using the Kubelka–Munk method [63]. The absorption edges were found to be 384, 384, 383 and 415 nm, which values correspond to the band gap energies of E_g = 3.23, 3.23, 3.24 and 2.99 eV for TNT400–TNT700, respectively. The E_g of 3.23-3.24 eV is typical for the anatase phase, whereas the decrease of the energy band gap to 2.99 eV is associated with the phase transformation from anatase to rutile, what was confirmed on a basis of the XRD patterns (Fig. 5).

3.3. Effect of calcination temperature on the photocatalytic activity of TNTs

In order to evaluate the photocatalytic activity of the as-received (TNT-0) and calcinated TNTs the photodegradation experiments with application of Acid Red 18 as a model compound were performed. For comparison, the photocatalytic activity of P25 under the same conditions was measured. The obtained results are presented in Figs. 7 and 8.

It can be clearly seen (Fig. 7) that the TNT-0 exhibited no photoactivity towards AR18 decomposition. During 5 h of irradiation the concentration of the azo dye remained practically constant and equal to the initial concentration. The obtained results are consistent with the photocatalytic behavior of TNTs observed by Yu et al. [44] and Qamar et al. [45]. The lack of photoactivity of the as-received TNTs could be attributed to their structure which was supposed to be $H_2Ti_2O_5{\cdot}H_2O$ (compare Section 3.1). Qamar et al. [45] concluded that since the titanate nanotubes do not contain TiO_2 phase, they cannot be used as photocatalysts for the destruction of organic pollutants in water. On the opposite, Costa et al. [53] reported a significant photoactivity of TNTs towards indigo carmine decomposition. However, the XRD analysis of the structure of TNTs obtained by the authors showed that the sample contained not only titanates, but also anatase. The presence of anatase phase might explain the photoactivity of the sample [53]. In view of the above, it could be concluded that TNTs composed of titanium acid, such as $H_2Ti_2O_5{\cdot}H_2O$, or titanates ($Na_2Ti_2O_5{\cdot}H_2O$) do not exhibit photocatalytic activity towards decomposition of organics in water.

Calcination of the TNTs resulted in an improvement of their photoactivity, as can be observed in Fig. 7. The reason for that was the formation of anatase structure under the heat treatment (Fig. 5). From the obtained results (Fig. 7) it can be clearly seen that the photoactivity of the samples was dependent on the calcination temperature. The least active photocatalysts towards AR18 decomposition were TNT400 and TNT500. The efficiency of AR18 decomposition in case of these two catalysts was comparable. After 5 h of irradiation the concentration of AR18 decreased for ca. 88% in case of TNT400 and 90% in case of TNT500. The most efficient photocatalyst towards the azo dye decomposition was that prepared at 600 °C. After 5 h of the process a complete decolorization of the solution was observed. Rising the calcination temperature up to 700 °C resulted in a decrease of the photoactivity of the sample. However, it should be noticed that the effectiveness of photodecomposition of AR18 in case of TNT700 was still higher than that observed for TNT400 and TNT500. Low photoactivity of the samples annealed at 400 and 500 °C might be attributed to their poor crystallinity (Fig. 5) with respect to anatase phase. The decrease of the photocatalytic activity of TNT700 compared to that of TNT600 was mainly associated with a partial transformation of highly photoactive anatase to poorly active rutile. The influence of the presence of $Na_2Ti_6O_{13}$ on the photocatalytic behaviour could probably be neglected. This conclusion could be supported by the results published by Torres-Martínez et al. [65] who found that single phase sodium hexatitanate exhibited very little photocatalytic activity towards Methylene Blue decomposition.

From Fig. 7 it can be also observed that although the heat treatment improved the photocatalytic activity of TNTs, it was lower than that of P25. Concentration of AR18 after 2 h of irradiation in the presence of P25 was about 0.7 mg/dm^3. In case of the most photoactive heat-treated TNTs (TNT600), similar decolorization was obtained after 4 h of the experiment.

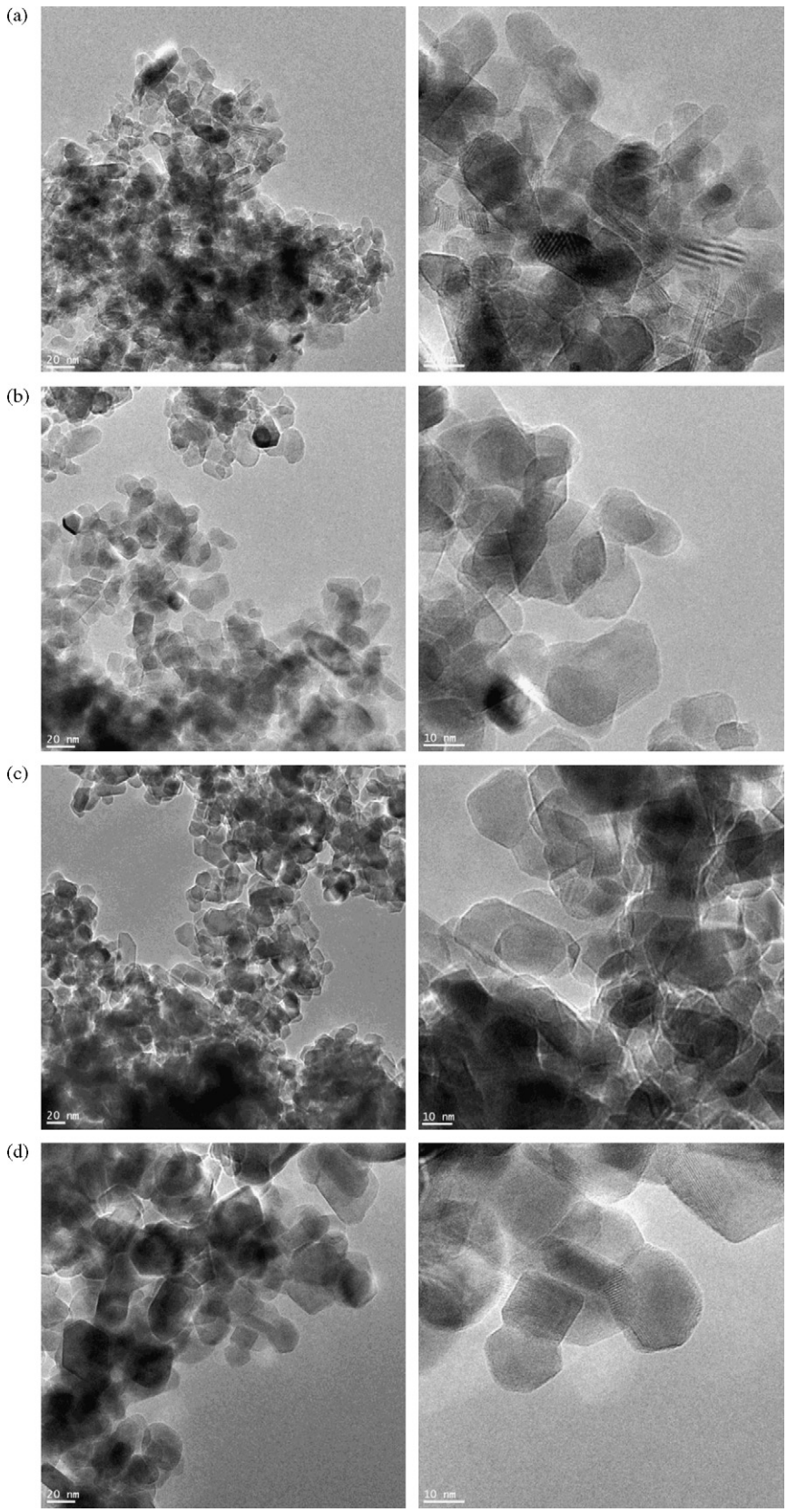

Fig. 6. TEM images of the titanate nanotubes calcinated at 400–700 °C: (a) TNT400; (b) TNT500; (c) TNT600; (d) TNT700.

The fading of the azo dye solution is associated with the cleavage of azo bonds (–N=N–) which are the most active bonds in the dye molecules. During the subsequent stages of photodegradation the cleavage of benzene and naphthalene rings followed by a series of oxidation steps takes place what further leads to the progressively lower molecular weight aliphatic acids and eventually to a complete mineralization to water, CO_2 and mineral salts (sulfates, nitrates, etc.) [68]. The overall reaction equation can be presented

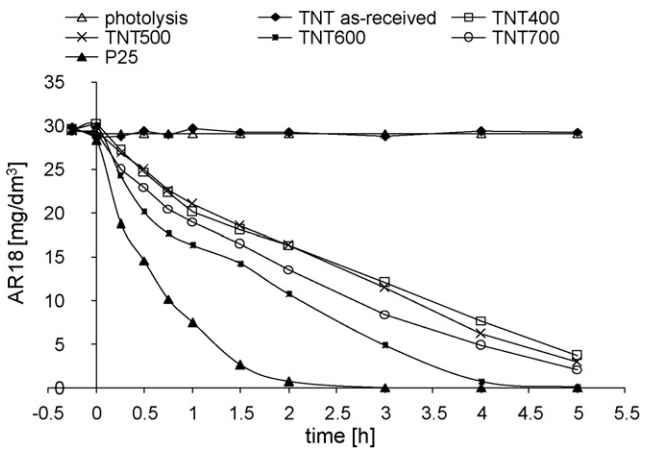

Fig. 7. Changes of AR18 concentration during photocatalytic decomposition with application of the as-received titanate nanotubes (TNT-0), thermally modified TNTs and P25. Process parameters: $c_0 = 30\ mg/dm^3$; catalyst loading, $0.3\ g/dm^3$; solution volume, $0.4\ dm^3$; reaction temperature, 25 °C.

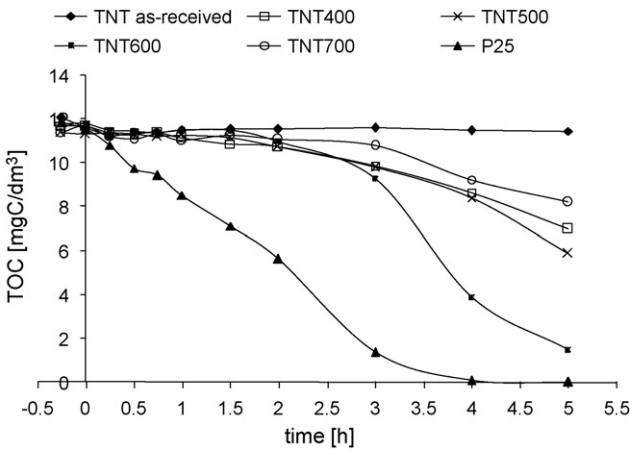

Fig. 8. Changes of TOC concentration during photocatalytic decomposition of AR18 with application of the of the as-received titanate nanotubes (TNT-0), thermally modified TNTs and P25. Process parameters: $c_0 = 30\ mg/dm^3$; catalyst loading, $0.3\ g/dm^3$; solution volume, $0.4\ dm^3$; reaction temperature, 25 °C.

as follows:

$$C_{20}H_{11}N_2Na_3O_{10}S_3 \rightarrow \text{aromaticintermediates}$$

$$\rightarrow \text{finalproducts}(CO_2, H_2O, SO_4^{2-}, NO_3^{-}, Na^{+})$$

Fig. 8 shows the effect of calcination temperature of TNTs on the efficiency of TOC removal during AR18 degradation. The changes of TOC concentration represent the effectiveness of mineralization of the model azo dye under the conditions applied.

It can be observed that the mineralization was less effective than decolorization. For the initial 2 h of irradiation the concentration of organic carbon remained, in fact, unchanged. The mineralization efficiency increased starting from the third hour of the experiment. Taking into account the results obtained at the end of the process, the efficiency of the mineralization could be put in the following order: TNT700 < TNT400 ≈ TNT500 < TNT600. The catalyst calcinated at 700 °C was the least effective in TOC degradation, although it exhibited higher effectiveness of decolorization of the solution than TNT400 and TNT500. Moreover, similarly as in case of AR18 decomposition (Fig. 7), the course of changes of TOC concentration for the samples prepared at 400 and 500 °C was almost the same. The highest mineralization efficiency was observed in case of TNT600. After 5 h of irradiation the concentration of TOC in the reaction mixture was $1.5\ mg/dm^3$.

For comparison, the results obtained with P25 are shown in Fig. 8. Similarly as in case of decolorization of the AR18 solution, P25 photocatalyst was found to be more active than the calcinated TNTs. Moreover, in contrast to the results obtained for the annealed TNTs, a continuous TOC removal can be observed in the presence of P25. This clearly shows that P25 was not only more efficient in decomposition of AR18, but also in its degradation. Unfortunately, it is impossible to compare the obtained results with the literature data, because the authors did not discuss mineralization of pollutants in the presence of calcinated TNTs. Evaluation of the mineralization efficiency during photocatalytic reaction is very important. Decolorization of the solution does not provide complete information on the effectiveness of degradation in the presence of a photocatalyst. The importance of determination of parameters such as TOC concentration could be proved on a basis of the results shown in Figs. 7 and 8. From Fig. 7 it can be found that decomposition of the dye started from the beginning of irradiation. However, the data presented in Fig. 8 clearly show that degradation in the presence of calcinated TNTs started after about 2 h of irradiation. This suggests that during the initial 2 h the breakage of the azo bond in the dye molecule took only place, what resulted in decolorization of the solution. Degradation of the by-products started significantly later.

As was mentioned earlier, the highest mineralization efficiency in case of the calcinated TNTs was observed for the sample annealed at 600 °C. The literature data concerning the effect of calcination temperature on photocatalytic activity of TNTs are inconsistent. For example, Zhang et al. [59] found that the photoactivity of titanate nanotubes towards degradation of propylene in air increased with increasing calcination temperature up to 500 °C and then decreased. Similar observations were reported by Yu et al. [44]. The authors investigated decomposition of acetone in air and found that the photocatalytic activity of the samples prepared at 400 and 500 °C were similar one to another and higher than that of the sample calcinated at 600 °C. Qamar et al. [45] reported that the highest activity towards amaranth degradation exhibited titanate nanotubes calcinated at 400 or 500 °C, depending on sodium content. On the opposite, Inagaki et al. [50] found that the highest rate constant of Methylene Blue degradation was obtained in case of TNTs heated at 600 °C, which data are consistent with the results obtained during the presented research. Different optimum calcination temperatures might be associated with various TNTs preparation conditions as well as different model compounds and reaction environments applied during the investigations. Amongst the factors associated with the preparation conditions, the temperature and time of the hydrothermal treatment, TNT precursor and washing step seem to be the most important. Other factors influencing the structure of the samples and, eventually, their photoactivity are conditions of the heat treatment (time, heating rate, static or flowing air, etc.). For example, the samples described in Refs. [44,45] were calcinated in air for 2 h. The TNTs used in the study presented in this paper were annealed in a muffle furnace for 1 h. Longer heat treatment time might result in a more significant crystal growth. Qamar et al. [45] reported that the TNTs calcinated at 600 °C for 2 h exhibited crystallite size of anatase of about 26 nm. The TNT600 sample, which was calcinated at 600 °C for 1 h contained anatase with crystallite size of 18 nm (compare Section 3.2). These data clearly show how the heat treatment conditions affect the sample properties. Next factor which could explain the inconsistencies between the results obtained in the presented research and the literature data is the environment of the photocatalytic reaction. For example, Yu et al. [44] reported about three times higher activity of calcinated TNTs compared to that of P25. The results presented in Figs. 7 and 8 clearly show that regardless of

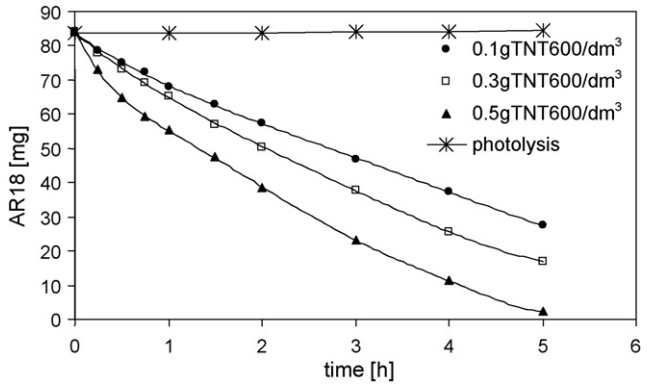

Fig. 9. Changes of the amount of AR18 in the feed solution during the photocatalytic decomposition conducted in the PMR. Process parameters: c_0 = 30 mg/dm^3; TNT600 catalyst loadings, 0.1–0.5 g/dm^3; initial solution volume, 2.9 dm^3; reaction temperature, 60 °C.

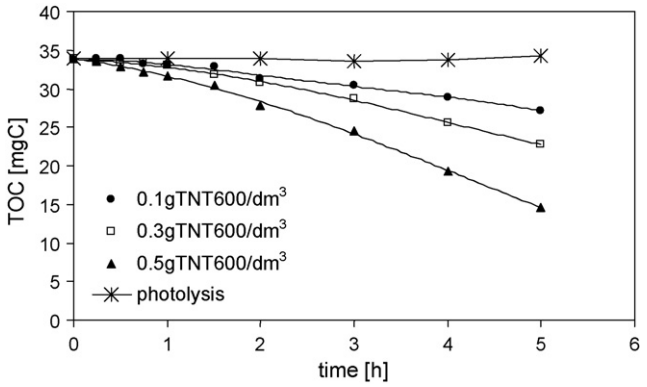

Fig. 10. Changes of the amount of TOC in the feed solution during the photocatalytic decomposition of AR18 conducted in the PMR. Process parameters: c_0 = 30 mg/dm^3; TNT600 catalyst loadings, 0.1–0.5 g/dm^3; initial solution volume, 2.9 dm^3; reaction temperature, 60 °C.

the heat treatment temperature, the photoactivity of the calcinated TNTs was lower than that of P25. These contrary results could be attributed to the reaction environment. Yu et al. [44] investigated photodecomposition of acetone vapor in air. The very high reaction rates compared to that obtained with P25 might be associated with the fact that the reaction was conducted in gaseous phase. The results presented in Figs. 7 and 8 were obtained during photocatalytic degradation of AR18 in water. In view of the above it could be concluded that the photocatalytic behaviour of calcinated TNTs strongly depends on the reaction conditions. Moreover, it could be supposed that the heat-treated TNTs have more potential applications in the reactions conducted in gaseous phase rather than in water.

3.4. Photocatalytic degradation of Acid Red 18 in a photocatalytic membrane reactor

The aim of this part of the research was the investigation on the possibility of application of the annealed TNTs in the PMR coupling photocatalysis and MD. The influence of catalyst loading on the effectiveness of AR18 degradation and the permeate quality was especially investigated. On a basis of the results presented in Section 3.3 the TNT600 was selected for further experiments in the PMR.

The photocatalytic degradation of AR18 in the PMR was conducted at the temperature of 60 °C. The TNT600 loading was 0.1, 0.3 or 0.5 g/dm^3 and the initial concentration of the model azo dye was 30 mg/dm^3. Changes of the mass of the dye in feed solution versus time of the hybrid process performance are presented in Fig. 9. Application of mass units (e.g. mg) instead of concentration units (e.g. mg/dm^3) is beneficial since the changes of dye concentration due to the feed volume reduction can be taken into consideration in this way. In the MD process the water vapor and volatile compounds present in warm feed are transported through the pores of the membrane and then condensed/dissolved directly in cold distillate. As a result, the volume of feed solution is continuously decreasing and the concentration of non-volatile compounds present in the solution is increasing. Therefore, in order to calculate the effectiveness of dye degradation in the discussed system, the reduction of feed volume should be taken into account. For this reason, the mass units instead of concentrations are shown in Fig. 9.

The obtained data (Fig. 9) show that AR18 was continuously decomposed in time of irradiation, regardless of TNT600 loading applied. The effectiveness of decolorization was increasing with increasing photocatalyst concentration. After 5 h of irradiation the amount of AR18 was lowered for ca. 67, 80 and 97% reaching the values of ca. 27, 17 and 2 mg, for TNT600 loadings of 0.1–0.5 g/dm^3, respectively.

Taking into consideration that decolorization of the solution does not provide complete information on the degradation efficiency, the TOC concentration was also monitored. Fig. 10 presents changes of the amount of organic carbon in the feed for different TNT600 loadings. The effectiveness of mineralization at the lowest catalyst concentration applied was very poor. After 5 h of irradiation the TOC value decreased for 20% only. In case of 0.3 gTNT600/dm^3 the mass of organic carbon decreased for ca. 27%. The highest efficiency of mineralization was obtained for 0.5 gTNT600/dm^3 (57%). The mass of TOC in feed solution after 5 h of the process was ca. 28, 23 and 15 mg for catalyst loadings of 0.1–0.5 g/dm^3, respectively.

It can be observed that for the catalyst concentrations of 0.1 and 0.3 g/dm^3 the amount of organic carbon during the first 1–1.5 h of irradiation remained unchanged and the mineralization began after 2 h of the process performance. In case of 0.5 gTNT600/dm^3 the mineralization started from the very beginning of irradiation. However, the rate of the removal of organic carbon during the initial 1.5 h of the process was significantly lower than during the next 3 h of the experiment.

As was mentioned earlier, amongst the organic by–products of the photodecomposition of azo dyes both, aromatic and aliphatic compounds are present. In order to determine the aliphatic acids formed during the photodecomposition of AR18 the IC analysis was performed. Fig. 11 shows the amounts of ionic forms of selected aliphatic acids in the feed after 5 h of decomposition of AR18. It

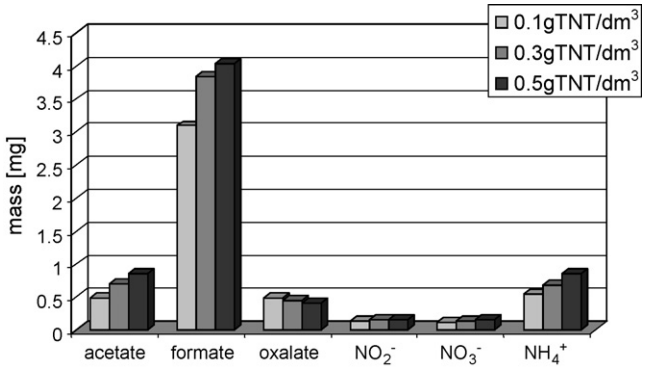

Fig. 11. The amount of selected ions in the feed solution after 5 h of photocatalytic degradation of AR18 in the PMR. Process parameters: c_0 = 30 mg/dm^3; TNT600 catalyst loadings, 0.1–0.5 g/dm^3; initial solution volume, 2.9 dm^3; reaction temperature, 60 °C.

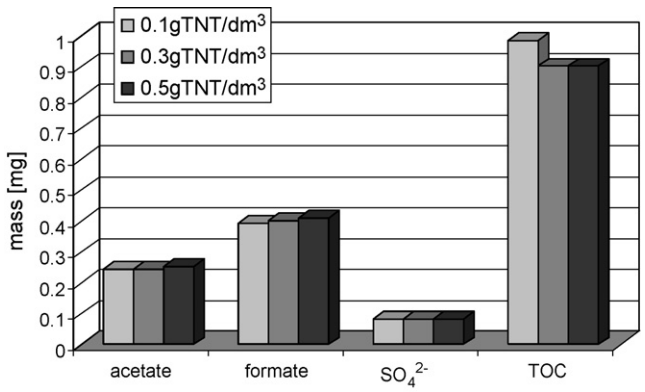

Fig. 12. The amount of selected ions and TOC in permeate after 5 h of photocatalytic degradation of AR18 in the PMR. Process parameters: c_0 = 30 mg/dm^3; TNT600 catalyst loadings, 0.1–0.5 g/dm^3; initial solution volume, 2.9 dm^3; reaction temperature, 60 °C.

can be observed that with increasing catalyst loading the amounts of the acids formed were increasing. Formic acid (HCOOH) was present at the highest concentration from all the acids monitored. The amount of $HCOO^-$ in the feed solution was in the range of 3.1–4.0 mg, for catalyst loadings of 0.1–0.5 g/dm^3, respectively. The amounts of acetate (CH_3COO^-) and oxalate ($HOOCCOO^-$) ions were significantly lower and ranged from 0.5–0.9 and 0.5–0.4 for 0.1–0.5 gTNT600/dm^3, respectively.

Fig. 11 presents also the amounts of selected inorganic ions being products (NO_3^-) or by-products (NO_2^- and NH_4^+) of AR18 degradation. It was found that the main form of nitrogen in the feed solution was NH_4^+. The amount of NH_4^+ was about five times higher than that of NO_3^-. This result might be associated with the process parameters applied. The temperature of the feed was high (60 °C) what restricted the solubility of oxygen in the solution. Thus, the O_2 concentration was probably too low to assure complete oxidation of NH_4^+ to NO_3^-. Except from nitrites, nitrates and ammonia, sulfates were also identified in the feed. The amount of SO_4^{2-} was increasing with increasing catalyst loading from ca. 26 to 43 mg for 0.1–0.5 gTNT600/dm^3.

The product of the hybrid photocatalysis-MD process; however, is not the feed solution, but distillate. Therefore, the quality of distillate was monitored during the process performance. The parameters measured were dye, TOC as well as organic and inorganic ions concentrations. It was found that, regardless of the TNT600 loading applied, the total amount of the dye remained on the feed side and its concentration in distillate amounted to 0 mg/dm^3. This was due to the fact that MD membrane is permeable for volatile compounds and water vapor only. AR18 is a non-volatile compound; therefore, it was not transported through the membrane. It is a significant advantage of the PMR utilizing MD. In case of the hybrid processes coupling photocatalysis and membrane techniques, which are described in the literature [1,19,29], a complete separation of dye molecules was not achieved.

Amongst the volatile compounds which passed through the MD membrane some organics were present. This conclusion was supported by the measurements of TOC concentration in distillate. Fig. 12 presents the amount of organic carbon in permeate at the end of the hybrid process (the dilution ratio of permeate in distillate was taken into account). No significant difference between the TOC concentration in permeate obtained with different catalyst loadings was observed. After 5 h of the process the mass of total organic carbon was about 0.9–1.0 mg what corresponded to 1.1–1.2 mgTOC/dm^3. The main volatile organic species present in permeate were formic and acetic acids (Fig. 12). Similarly, as in case of TOC concentration, no significant effect of TNT600 loading on the amount of acetate and formate ions in permeate was observed. The amount of $HCOO^-$ was higher than that of CH_3COO^-, what was reasonable since the amount of formic acid in the feed solution was higher than that of acetic acid. The concentrations of formic and acetic acids in permeate, regardless of catalyst loading applied, were about 0.4 and 0.2 mg/dm^3 what corresponded to the masses of 0.5 and 0.3 mg, respectively.

From Fig. 12 it can be also found that permeate contained very low amounts of sulfates. Sulfuric acid exhibits very low volatility, therefore SO_4^{2-} should not be transported through the MD membrane. An explanation for the presence of SO_4^{2-} in permeate might be droplets entrainment, i.e. mist flow instead of vapor (gas) flow.

Another parameters monitored in distillate were conductivity and pH. Electrical conductivity (σ) corresponds to the ionic activity of a solution in term of its capacity to transmit current. Conductivity of distillate could be regarded as a measure of the amount of ionic products and by-products formed during photodegradation of AR18, which were transported through the MD membrane. It was found that the conductivity of distillate was in the range of 2.3–3 μS/cm (vs. 1 μS/cm measured in water used for preparation of the solutions) and was the highest for the highest catalyst loading applied. Since the amounts of volatile organic compounds represented by TOC were almost independent on the catalyst loading (Fig. 12), it could be supposed that an increase of conductivity with increasing TNT600 concentration was associated with the transport of CO_2 through the membrane pores. Carbon dioxide dissolves in water thus forming carbonic acid. H_2CO_3 is a weak acid which dissociates into H^+ and HCO_3^- ions. These ions, on the contrary to gaseous CO_2, contribute to the electrical conductivity of distillate. However, at pH < 7, the concentration of CO_2 is significantly higher, than that of bicarbonate ions, therefore the observed increase of conductivity with increasing TNT600 loading was not very significant.

The pH of distillate slightly decreased from pH 5.7 at the beginning of the process to ca. pH 5.2 at the end of experiment. These changes in the pH value suggest that some acidic compounds were transported through the membrane. On a basis of the results presented in Fig. 12 it could be supposed that the main species responsible for a decrease of pH of distillate were volatile organic acids and sulfuric acid. Moreover, the effect of carbonic acid should be also taken into consideration.

The obtained results clearly show that the product of the hybrid photocatalysis–MD process was high quality water. Application of MD ensured high efficiency of separation of the dye as well as products of its degradation. Moreover, the MD process was very effective in rejection of photocatalyst particles, what was found on a basis of turbidity measurement. For example, the turbidity of feed solution at 0.5 gTNT600/dm^3 was 1683 NTU, whereas the turbidity of distillate was 0.4 NTU. It should be mentioned; however, that MD is still the process under development and, therefore, the pressure driven membrane processes have more potential full scale applications than MD. Another obstacle in application of MD in PMRs seems to be the permeate flux, which is lower than that in the pressure driven membrane processes. However, at low fluxes the hydraulic retention times, i.e. the times of residence of the contaminants in the reactor are longer and the photodegradation is more effective.

4. Conclusions

The presented studies were focused on preparation of thermally modified titanate nanotubes and their application for azo dye Acid Red 18 removal in a photocatalytic membrane reactor coupling photocatalysis and membrane distillation.

The as-received TNTs (TNT-0) prepared by the hydrothermal method were found to be not active in the photocatalytic decomposition of AR18 under UV light. The lack of photoactivity of the as-received TNTs could be attributed to their structure which was

supposed to be $H_2Ti_2O_5 \cdot H_2O$. Thus, it can be concluded that unmodified TNTs have no potential application in photocatalytic removal of organic compounds, such as azo dyes, from water.

Thermal post-treatment of titanate nanotubes improved significantly their photoactivity, what can be attributed to the formation of anatase phase. The photocatalytic activity of modified TNTs increased with increasing calcination temperature from 400 to 600 °C. The observed improvement of the effectiveness of AR18 degradation was associated with the anatase crystal growth in the thermally treated samples. Rising the heat treatment temperature up to 700 °C led to a decrease in the TNTs photoactivity, what was due to a partial transformation of anatase to rutile.

Although the post-treatment of TNTs resulted in an improvement of their photocatalytic activity, the effectiveness of degradation of AR18 in the presence of calcinated TNTs was lower than in case of P25, regardless of the annealing temperature used.

However, it should be stressed that the obtained results significantly contribute to the knowledge on photocatalytic applications of titanate nanotubes. The literature data in this area are inconsistent and misleading. Since numerous papers show that the as-received or heat-treated TNTs could exhibit very high photocatalytic activity in degradation of organic compounds, there is a need to verify these data. The results obtained during the presented studies show that one must be very careful when selecting TNTs or annealed TNTs as a photocatalytic material for removal of organic compounds from water.

The TNTs calcinated at 600 °C were applied for photocatalytic degradation of AR18 in the PMR. After 5 h of the hybrid process the amount of AR18 in the feed solution was lowered for ca. 67, 80 and 97% for TNT600 loadings of 0.1–0.5 g/dm^3, respectively. The mineralization of the organic compounds was significantly lower than the decolorization of the solution. The amount of TOC after 5 h of irradiation decreased for 20, 27 and 57%, for 0.1–0.5 gTNT600/dm^3, respectively. Amongst products and by-products of AR18 photodegradation organic acids (formic, acetic and oxalic) and inorganic ions (nitrite, nitrate, ammonia and sulfate) were detected. The main form of nitrogen in the feed was NH_4^+, what was associated probably with a low concentration of oxygen in the solution under the conditions applied (60 °C).

Although the photocatalytic activity of TNT600 was lower compared to that of P25, the product of the hybrid process (distillate) was high quality water. The conductivity of distillate ranged from 2.3 to 3 μS/cm. The TOC concentration in permeate was in the range of 1.1–1.2 mgC/dm^3. The presence of organic carbon in the permeate was attributed mainly to the transport of volatile organic acids (formic and acetic) through the membrane pores.

The hybrid photocatalysis-MD system was found to be a promising method of removal of organic compounds such as azo dyes from water.

Acknowledgements

The presented research is co-financed by the Foundation for Polish Science, which has been supported by a grant from Iceland, Liechtenstein and Norway through the EEA Financial Mechanism.

References

[1] R. Molinari, L. Palmisano, E. Drioli, M. Schiavello, J. Membr. Sci. 206 (2002) 399.
[2] J.-T. Jung, J.-O. Kim, W.-Y. Choi, Mater. Sci. Forum. 544–545 (2007) 95.
[3] J. Ryu, W. Choi, K.-H. Choo, Water Sci. Technol. 51 (2005) 491.
[4] J. Fu, M. Ji, Z. Wang, L. Jin, D. An, J. Hazard. Mater. 131 (2006) 238.
[5] R. Thiruvenkatachari, T.-O. Kwon, I.-S. Moon, Sep. Sci. Technol. 40 (2005) 2871.
[6] S.S. Chin, T.M. Lim, K. Chiang, A.G. Fane, Desalination 202 (2007) 253.
[7] T.E. Doll, F.H. Frimmel, Water Res. 39 (2005) 847.
[8] M.J. Rivero, S.A. Parsons, P. Jeffrey, M. Pidou, B. Jefferson, Water Sci. Technol. 53 (2006) 173.
[9] X. Huang, Y. Meng, P. Liang, Y. Qian, Sep. Purif. Technol. 55 (2007) 165.
[10] P. Cui, X. Zhao, M. Zhou, L. Wang, Chin. J. Catal. 27 (2006) 752.
[11] P. Le-Clech, E.-K. Lee, V. Chen, Water Res. 40 (2006) 323.
[12] X.Z. Li, Y.G. Zhao, Water Sci. Technol. 39 (1999) 249.
[13] K.-W. Choo, D.-I. Chang, K.-W. Park, M.-H. Kim, J. Hazard. Mater. 152 (2008) 183.
[14] H.K. Shon, S. Phuntsho, S. Vigneswaran, Desalination 225 (2008) 235.
[15] M.-C. Chang, R.-Y. Horng, H. Shao, Y.-J. Hu, Filtration 6 (2006) 340.
[16] M.J. Benotti, B.D. Stanford, E.C. Wert, S.A. Snyder, Water Res. 43 (2009) 1513.
[17] L. Erdei, N. Arecrachakul, S. Vigneswaran, Sep. Purif. Technol. 62 (2008) 382.
[18] K. Sopajaree, S.A. Qasim, S. Basak, K. Rajeshwar, J. Appl. Electrochem. 29 (1999) 533.
[19] K. Sopajaree, S.A. Qasim, S. Basak, K. Rajeshwar, J. Appl. Electrochem. 29 (1999) 1111.
[20] R. Molinari, M. Mungari, E. Drioli, A. Di Paola, V. Loddo, L. Palmisano, M. Schiavello, Catal. Today 55 (2000) 71.
[21] S.A. Tsarenko, V.M. Kochkodan, A.O. Samsoni-Todorov, V.V. Goncharuk, Colloid J. 68 (2006) 341.
[22] D. Sun, T.T. Meng, T.H. Loong, T.J. Hwa, Water Sci. Technol. 49 (2004) 103.
[23] S.-A. Lee, K.-H. Choo, C.-H. Lee, H.-I. Lee, T. Hyeon, W. Choi, H.-H. Kwon, Ind. Eng. Chem. Res. 40 (2001) 1712.
[24] J. Fu, M. Ji, Y. Zhao, L. Wang, Sep. Purif. Technol. 50 (2006) 107.
[25] R. Molinari, M. Borgese, E. Drioli, L. Palmisano, M. Schiavello, Catal. Today 75 (2002) 77.
[26] R. Molinari, C. Grande, E. Drioli, L. Palmisano, M. Schiavello, Catal. Today 67 (2001) 273.
[27] R. Molinari, F. Pirillo, V. Loddo, L. Palmisano, Catal. Today 118 (2006) 205.
[28] V. Augugliaro, E. García-López, V. Loddo, S. Malato-Rodríguez, I. Maldonado, G. Marcì, R. Molinari, L. Palmisano, Sol. Energy 79 (2005) 402.
[29] R. Molinari, F. Pirillo, M. Falco, V. Loddo, L. Palmisano, Chem. Eng. Process. 43 (2004) 1103.
[30] R. Molinari, A. Caruso, P. Argurio, T. Poerio, J. Membr. Sci. 319 (2008) 54.
[31] K. Azrague, P. Aimar, F. Benoit-Marquié, M.T. Maurette, Appl. Catal. B 72 (2006) 197.
[32] G. Camera-Roda, F. Santarelli, J. Sol. Energy Eng. 129 (2007) 68.
[33] S. Mozia, M. Tomaszewska, A.W. Morawski, Appl. Catal. B 59 (2005) 133.
[34] S. Mozia, A.W. Morawski, Catal. Today 118 (2006) 181.
[35] S. Mozia, M. Tomaszewska, A.W. Morawski, Desalination 198 (2006) 183.
[36] S. Mozia, M. Tomaszewska, A.W. Morawski, Catal. Today 129 (2007) 3.
[37] S. Mozia, A.W. Morawski, M. Toyoda, M. Inagaki, Sep. Purif. Technol. 63 (2008) 386.
[38] S. Mozia, A.W. Morawski, M. Toyoda, M. Inagaki, Desalination 241 (2009) 97.
[39] S. Mozia, A.W. Morawski, M. Toyoda, T. Tsumura, Chem. Eng. J. 150 (2009) 152.
[40] S. Mozia, A.W. Morawski, J. Adv. Oxid. Technol. 12 (2009) 111.
[41] T. Kasuga, M. Hiramatsu, A. Hoson, T. Sekino, K. Niihara, Langmuir 14 (1998) 3160.
[42] T. Kasuga, M. Hiramatsu, A. Hoson, T. Sekino, K. Niihara, Adv. Mater. 11 (1999) 1307.
[43] H.H. Ou, S.-L. Lo, Sep. Purif. Technol. 58 (2007) 179.
[44] J. Yu, H. Yu, B. Cheng, C. Trapalis, J. Mol. Catal. A 249 (2006) 135.
[45] M. Qamar, C.R. Yoon, H.J. Oh, N.H. Lee, K. Park, D.H. Kim, K.S. Lee, W.J. Lee, S.J. Kim, Catal. Today 131 (2008) 3.
[46] K.V. Baiju, S. Shukla, S. Biju, M.L.P. Reddy, K.G.K. Warrier, Mater. Lett. 63 (2009) 923.
[47] T. Tachikawa, S. Tojo, M. Fujitsuka, T. Sekino, T. Majima, J. Phys. Chem. B 110 (2006) 14055.
[48] A. Nakahira, W. Kato, M. Tamai, T. Isshiki, K. Nishio, J. Mater. Sci. 39 (2004) 4239.
[49] M.W. Xiao, L.S. Wang, X.J. Huang, Y.D. Wu, Z. Dang, J. Alloys Compd. 470 (2009) 486.
[50] M. Inagaki, N. Kondo, R. Nonaka, E. Ito, M. Toyoda, K. Sogabe, T. Tsumura, J. Hazard. Mater. 161 (2009) 1514.
[51] J. Geng, D. Yang, J. Zhu, D. Chen, Z. Jiang, Mater. Res. Bull. 44 (2009) 146.
[52] F. Jiang, S. Zheng, Z. Zheng, Z. Xu, Y. Wang, J. Environ. Sci. 18 (2006) 783.
[53] L.L. Costa, A.G.S. Prado, J. Photochem. Photobiol. A: Chem. 201 (2009) 45.
[54] Ch.-K. Lee, Ch.-C. Wang, M.-D. Lyu, L.-Ch. Juang, S.-S. Liu, S.-H. Hung, J. Colloid Int. Sci. 316 (2007) 562.
[55] H. Kochkar, N. Lakhdhar, G. Berhault, M. Bausach, A. Ghorbel, J. Phys. Chem. C 113 (2009) 1672.
[56] R. Ma, Y. Bando, T. Sasaki, J. Phys. Chem. B 108 (2004) 2115.
[57] J.A. Toledo-Antonio, S. Capula, M. Antonia Cortés-Jácome, C. Angeles-Chávez, E. López-Salinas, G. Ferrat, J. Navarrete, J. Escobar, J. Phys. Chem. C 111 (2007) 10799.
[58] C.-C. Tsai, H. Teng, Chem. Mater. 18 (2006) 367.
[59] M. Zhang, J. Zhensheng, J. Zhang, X. Guo, J. Yang, W. Li, X. Wang, Z. Zhang, J. Mol. Catal. A 217 (2004) 203.
[60] Q. Chen, G.H. Du, S. Zhang, L.-M. Peng, Acta Crystallogr. B58 (2002) 587.
[61] E. Morgado Jr., M.A.S. de Abreu, G.T. Moure, B.A. Marinkovic, P.M. Jardim, A.S. Araujo, Chem. Mater. 19 (2007) 665.
[62] R. Ma, Y. Bando, T. Sasaki, Chem. Phys. Lett. 380 (2003) 577.
[63] N. Todorova, T. Giannakopoulou, G. Romanos, T. Vaimakis, J. Yu, C. Trapalis, Int. J. Photoenergy (2008), doi:10.1155/2008/534038, 9 pages, Article ID 534038.
[64] N. Wang, H. Lin, J. Li, X. Yang, B. Chi, C. Lin, J. Alloys Compd. 424 (2006) 311.
[65] L.M. Torres-Martínez, I. Juárez-Ramírez, K. Del Ángel-Sánchez, L. Garza-Tovar, A. Cruz-López, G. Del Ángel, J. Sol Gel Sci. Technol. 47 (2008) 158.
[66] C. Su, B.-Y. Hong, C.-M. Tseng, Catal. Today 96 (2004) 119.
[67] L. Zhang, H. Lin, N. Wang, C. Lin, J. Li, J. Alloys Compd. 431 (2007) 230.
[68] I.K. Konstantinou, T.A. Albanis, Appl. Catal. B 49 (2004) 1.